Journal of the Korean Physical Society, Vol. 65, No. 2, July 2014, pp. 145∼150

Charge Transport at High Temperatures in Solution-processed Zinc-tin-oxide Thin-film Transistors

Kyeong Min Yu and Byung Seong Bae
Department of Display Engineering, Hoseo University, Asan 336-795, Korea

Myunghee Jung
Digital Media Engineering, Anyang University, Anyang 430-714, Korea

Eui-Jung Yun*
Department of Information Communication Engineering, Hoseo University, Asan 336-795, Korea

(Received 14 January 2014, in final form 19 February 2014)

We report charge transport studies at temperatures in the range of 303 − 402 K for solution-deposited amorphous zinc-tin-oxide (a-ZTO) thin-film transistors (TFTs) operating in the sub-threshold region. The developed TFTs, which had a non-patterned bottom gate and top contact structure, employed a heavily-doped Si wafer and a SiO_2 as a gate electrode and a gate insulator layer, respectively. In a-ZTO, the trap activation energy (E_{TAC}) was estimated using the Maxwell-Boltzmann approximation. The decreasing E_{TAC} with increasing gate-voltage-induced sheet carrier density (n_s) in the a-ZTO channel can be understood as being due to a shift of the Fermi level (E_F) toward the conduction band edge (E_C) with increasing gate voltage. Samples with low n_s, which exhibited thermally-activated behavior, revealed multiple trap and release phenomena. In samples with high n_s, on the other hand, we observed decreasing mobility/conductivity with increasing temperature at temperatures higher than 348 K. This suggests that the E_{TAC} can drop to zero, implying a shift of E_F beyond E_C, where the crossover from the thermal activation to band transport is observed. The temperature-dependent characteristics also revealed that the density of subgap trap states at E_F exhibited thermally-activated behavior with an activation energy of 0.7 eV, suggesting that subgap trap states existed near 0.7 eV below the E_C.

PACS numbers: 61.43.Dq, 73.40.Qv, 73.50.-h, 85.30.Tv
Keywords: Charge transport, Solution-deposited amorphous zinc-tin-oxide (a-ZTO) thin-film transistors, Maxwell-Boltzmann approximation, Multiple trap and release, Conduction band edge
DOI: 10.3938/jkps.65.145

I. INTRODUCTION

Solution-processed amorphous zinc-tin-oxide (a-ZTO) thin films have, nowadays, attracted much attention as active layers in the fabrication of low-cost roll-to-roll printed thin film transistors (TFTs) because of their simplicity, low-cost, high throughput, and non-toxicity [1–8]. For low temperatures ranging from 77 to 300 K, the TFTs with a-ZTO active material also have very interesting charge transport mechanisms, ranging from thermally activated transport at low carrier densities in the saturation (on) region [9] or in the subthreshold region [10] to band transport at large carrier densities in the saturation region [2, 9]. Knowing the charge transport mechanism and the band structure are important to enable successful device simulation and device stability studies [10, 11]. Hence, a comprehensive picture of charge transport in this unique a-ZTO material needs to be developed.

Transport mechanisms in this kind of material have been explored by using various measurement techniques, such as time-of-flight (TOF) [12], Hall-effect [13], and field-effect transistor (FET) [9, 14] methods. Two well-known models to describe the transport mechanism are the multiple trap and release (MTR) [15] and the Monroe [16] models. These models assume that amorphous Si (a-Si) and most amorphous oxide semiconductors in thin-film form have a high density of localized trap-states in the forbidden gap between the conduction and the valence bands. These models have also been used to describe transport in a-Si for many decades and are applicable to a-ZTO. There have been limited studies of charge transport in a-ZTO [9,10]. Moreover, there have

*E-mail: ejyun@hoseo.edu; Tel: +82-41-540-5675; Fax: +82-41-540-5587

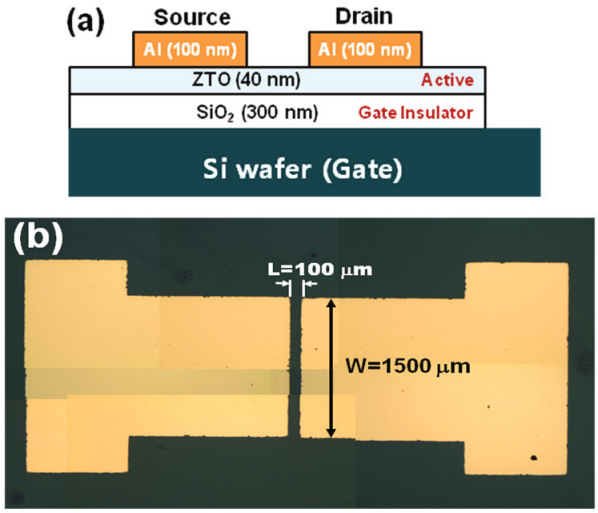

Fig. 1. (Color online) (a) Schematic cross-sectional view and (b) photographic top view of a solution-deposited a-ZTO TFT developed in this work: W = 1500 μm and L = 100 μm.

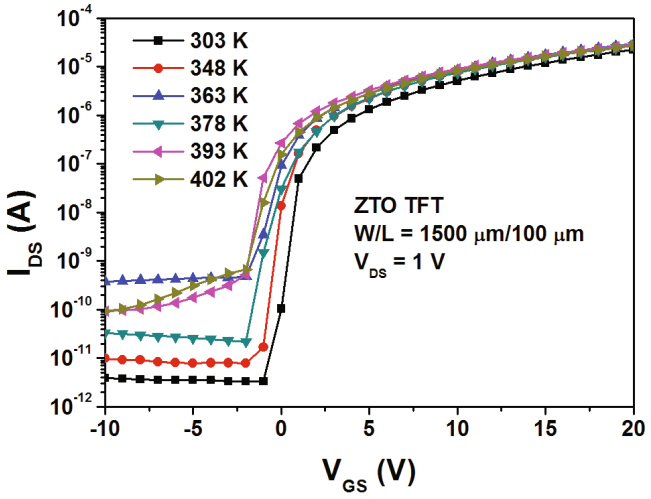

Fig. 2. (Color online) Typical temperature-dependent $I_{DS} - V_{GS}$ transfer characteristics of solution-processed a-ZTO TFTs measured at V_{DS} = 1V for temperatures ranging from 303 to 402 K.

been no clear reports of band transport or documentation of conduction band edge behavior in any solution-processed amorphous semiconductor. Thus, in this research, we demonstrated the detailed charge transport properties of solution-deposited a-ZTO based TFTs especially at various temperatures ranging from 303 to 402 K in the subthreshold region.

II. EXPERIMENTS

The fabrication process of TFTs is as follows: The precursor solution for the ZTO active layer was synthesized with a sol-gel method by dissolving zinc acetate dihydrate and tin chloride powders in 2-methoxyethanol, which was stabilized with acetylacetone. The concentration of the precursor solution was 0.3 M with a Zn/Sn molar ratio of 1. The precursor solution was stirred for 8 hrs at 80 °C, filtered through a 0.2 μm membrane syringe filter, and spin-coated at 4000 rpm for 50 sec on the top of a 300-nm-thick SiO_2 gate dielectric layer thermally-grown on a heavily-doped p-type Si gate electrode. Then, the ZTO prebake process was carried out at 100 °C for 1.5 min. on a hot plate in air to evaporate solvent. The precursor film was then converted to a 40-nm-thick ZTO active layer by annealing at 600 °C for 1 hr in a furnace. To fabricate TFTs, we deposited 100nm Al source and drain electrodes through a shadow mask by using a thermal evaporator.

Figures 1(a) and (b) show a schematic cross-sectional view and a photographic top view, respectively, of a typical solution-deposited a-ZTO TFT developed in this study. As shown in Fig. 1, the TFTs have a non-patterned bottom gate and a top contact structure. The channel width (W) and the channel length (L) were 1500 μm and 100 μm, respectively.

The subthreshold transfer and output characteristics of a-ZTO-based TFTs were measured at temperatures ranging from 303 to 402 K in a darkened probe box in air by using two Keithley 2400 source meters for a DC voltage source and a Keithley 6485 picoammeter for current measurements. Two-terminal measurements involving the use of source and drain electrodes were carried out after the TFTs had been placed on a hot plate. In order to describe the detailed charge transport properties of solution-deposited a-ZTO based TFTs, we observe a range of charge transport phenomena depending upon the charge density in the channel and the temperature.

III. RESULTS AND DISCUSSION

Figure 2 shows the typical temperature-dependent drain-to-source current versus gate-to-source voltage ($I_{DS} - V_{GS}$) transfer characteristics of the solution-processed ZTO TFTs. All measurements were performed with drain-to-source voltage (V_{DS}) fixed at 1 V, which is in the subthreshold region, and various temperatures ranging from 303 to 402 K were applied. The slope of the sub-threshold swing (SS), which describes the change in the V_{GS} that should be applied to devices in order to increase the I_{DS} an order of magnitude, of the same devices used in Fig. 2 was also obtained from the inverse slope of the curve in Fig. 2 by making use of [17,18]

$$SS = \left[\frac{\partial(\log I_{DS})}{\partial V_{GS}}\right]^{-1}. \quad (1)$$

If $V_{GS} - V_{ON} < V_{DS}$, then the device operates in the subthreshold mode, and the linear mobility, μ_{lin}, is cal-

Table 1. Summary of important device parameters of solution-deposited ZTO-based TFTs, which were obtained from the results in Fig. 2 by making use of Eqs. (1) and (2).

Temperature used for measurement (K)	SS (V/decade)	V_{ON} (V)	at $\mu_{lin}{}^{a)}$ $V_{GS}-V_{ON}=21$ V (cm^2/Vs)	$I_{DS\,off}$ (A)	$I_{on/off}$
303	0.48	−1	13.1	3.35×10^{-12}	6.64×10^{6}
348	0.51	−2	16.0	7.95×10^{-12}	3.63×10^{6}
363	0.58	−2	15.7	4.75×10^{-10}	6.25×10^{4}
378	0.64	−2	14.5	2.17×10^{-11}	1.24×10^{6}
393	0.74	−2	14.5	5.22×10^{-10}	5.48×10^{4}
402	0.85	−2	13.9	6.66×10^{-10}	4.05×10^{4}

a) It increases with increasing value of $V_{GS}-V_{ON}$.

culated from

$$\mu_{lin}=\frac{\partial I_{DS}}{\partial V_{GS}}\frac{L}{W}\frac{1}{C_{SiO_2}}\frac{1}{V_{DS}}, \tag{2}$$

where C_{SiO2} = 11.5 nF/cm^2 is the capacitance per unit area of the SiO_2 dielectric measured with a metal-insulator-metal structure. Table 1 summarizes important device parameters of solution-processed ZTO-based TFTs, which were obtained from the results in Fig. 2 by making use of Eqs. (1) and (2). As shown in Fig. 2 and Table 1, with increasing measurement temperature, the *SS* and the I_{DS} at the off-state (I_{off}) increased and the on-off ratio ($I_{on/off}$) decreased. The onset voltage (V_{ON}) was also shifted negatively for temperatures greater than 340 K. The V_{ON} is defined as the V_{GS} at which the mobile carriers start to accumulate in the channel and the I_{DS} starts to increase. Here, we used the V_{ON} rather than the threshold voltage (V_{th}) because the V_{ON} is mainly determined by trapped charges whereas shifts in the V_{th} in TFTs can be related to changes in many more physical parameters such as the *SS* and the mobility [19].

The μ_{lin} values derived from the transfer curves shown in Fig. 2 by using Eq. (2) are illustrated in Fig. 3 as a function of V_{GS} $-V_{ON}$ for temperatures ranging from 303 to 402 K for the a-ZTO TFTs. The applied V_{GS} was adjusted by using the V_{ON} to ensure that mobilities at various V_{GS} values could be accurately calculated [9]. As shown in Fig. 3, the linear mobility values increase with increasing $V_{GS}-V_{ON}$. In these a-ZTO TFTs, we also observe that the room-temperature μ_{lin} is high, around 13 cm^2/Vs.

The temperature dependence of the μ_{lin} data obtained from the curves shown in Fig. 3 is illustrated in Fig. 4(a) for different values of $V_{GS}-V_{ON}$. Here, the gate-voltage-dependent carrier density (per unit area) of band-tail trap states, which is the sheet carrier concentration, n_s

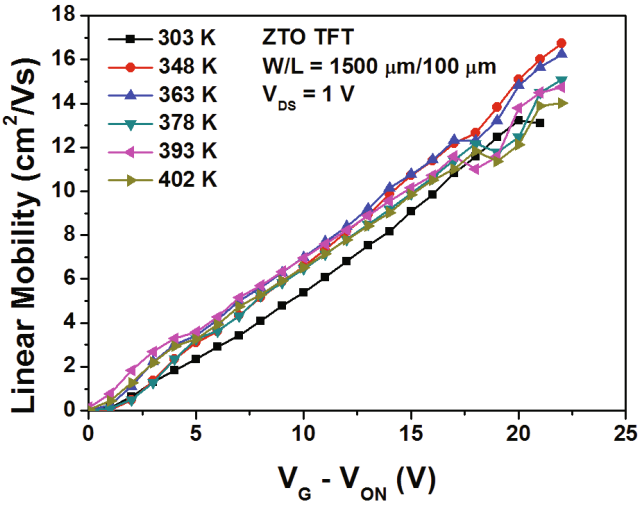

Fig. 3. (Color online) Linear mobilities (μ_{lin}) at various temperatures as functions of $V_{GS}-V_{ON}$ estimated with Eq. (2) from the transfer curves for the solution-processed a-ZTO TFTs shown in Fig. 2. The μ_{lin} increases with increasing $V_{GS}-V_{ON}$.

(= nt_{ch}), is defined as [10,20]:

$$n_s=nt_{ch}=\frac{C_{SiO_2}(V_{GS}-V_{ON})}{q}, \tag{3}$$

where n is the V_{GS}-induced charge carrier (volume) density, q is the charge of an electron, and t_{ch} is the estimated thickness of the ZTO conductive channel (∼3 nm). Then, the temperature and the $V_{GS}-V_{ON}$ dependences of the linear conductivity (σ_{lin}) data can be also obtained from the curves shown in Fig. 4(a) by using Eq. (3) and the relation of $\sigma_{lin}=nq\mu_{lin}$ and are shown in Fig. 4(b). As shown in Fig. 4, the thermally-activated behavior, which shows an increasing mobility with increasing temperature, is visible up to the $V_{GS}-V_{ON}$ value of 10 V.

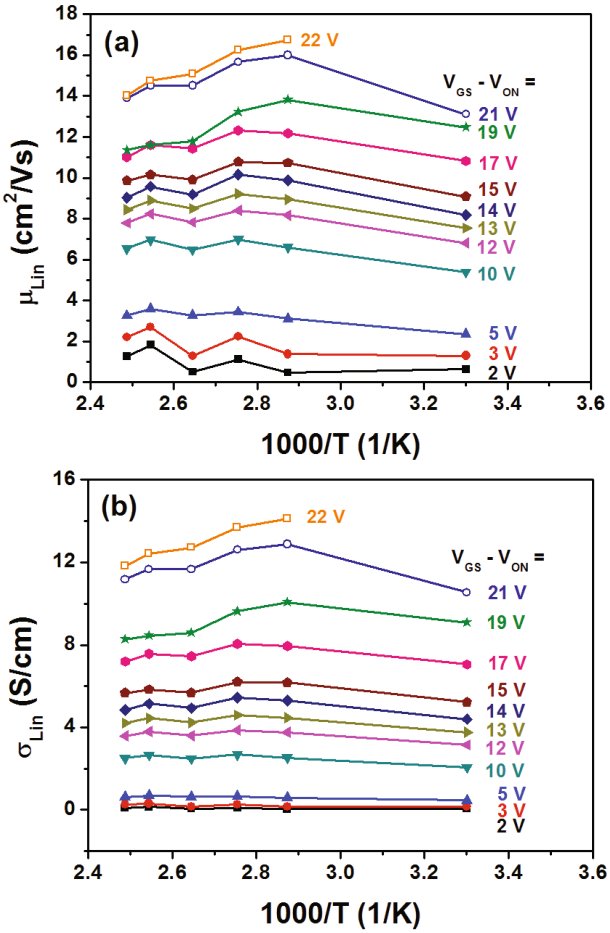

Fig. 4. (Color online) Temperature and $V_{GS} - V_{ON}$ dependence of (a) the linear mobility (μ_{lin}) and (b) the linear conductivity (σ_{lin}) data obtained from the curves shown in Fig. 3 by using Eq. (3) and the relation $\sigma_{lin} = nq\mu_{lin}$. A crossover from the thermal activation to band-like transport is observed in the sample at high $V_{GS} - V_{ON}$ (> 12 V).

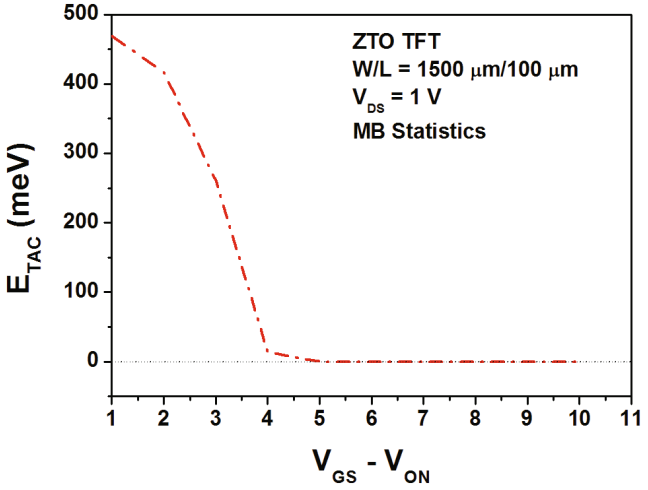

Fig. 5. (Color online) Characteristics of the E_{TAC} versus $V_{GS} - V_{ON}$ for the case of linear mobilities obtained from the curves shown in Fig. 4 by using Maxwell-Boltzmann (MB) statistics expressed in Eq. (3). The dotted line at $E_{TAC} = 0$ indicates the conduction band edge, E_C.

The MTR model [15] can apply to materials with localized states that are energetically close to a transport band edge (conduction band edge; E_C) above which band transport occurs and below which all states are trap states, such as a-ZTO. For charge carriers that are excited from localized states into the extended states beyond the mobility edge (E_C), the temperature-dependent mobility can be estimated with [15]

$$\mu_{eff} = \mu_0 \alpha e^{-E_{TAC}/k_B T} = \mu_0 \alpha e^{-(E_C - E_t)/k_B T} \quad (4)$$

by using Maxwell-Boltzmann (MB) statistics. Here, μ_0 is the drift mobility in the transport band, α is a constant related to the ratio of the number of extended states at the E_C (N_c) to the number of localized states (N_t), and $E_{TAC} = E_C - E_t$ is the energetic difference between the E_C and the trap energy (E_t), which is equivalent to the trap activation energy, and $k_B T$ is the thermal energy. A common practice is to calculate the E_{TAC} by using MB statistics for charge transport in various materials that follow the MTR model.

Equation (4) was fitted to data sets for the behaviors of the linear mobilities derived from the transfer curves as a function of $V_{GS} - V_{ON}$ for various temperatures for the a-ZTO TFTs (see Fig. 4) and to mobility measurements at the V_{DS} value of 1 V. This results in the characteristics of E_{TAC} versus $V_{GS} - V_{ON}$ shown in Fig. 5. As shown in Fig. 5 and Eq. (3), the E_{TAC} decreases with increasing value of $V_{GS} - V_{ON}$ and, thus, n_s and drops to zero at $n_s = 7.2 \times 10^{11}$ cm^{-2} for $V_{GS} - V_{ON} = 10$ V (estimated using Eq. (3)). The low energies less than 470 meV involved suggest that a hopping mechanism is unlikely to be the process underlying the charge carrier transport. Describing the shallow traps as being similar to shallow donor levels is more reasonable. In that sense, the decreasing E_{TAC} with increasing n_s can be understood as being due to a shift of the Fermi level (E_F), in accordance with the MTR model: The higher the applied V_{GS}, the larger the n_s is, which in turn moves the E_F closer to the E_C ($E_{TAC} = 0$ in Fig. 5) [20,21]. This facilitates the thermal release of electrons into the conduction band and, hence, causes an increasing time-averaged concentration of charge carriers in the conduction band. In this region, transport is thermally-activated. For $n_s > 7.2 \times 10^{11}$ cm^{-2}, the E_F level is above the E_C, and a majority of charge is in the extended states. In this region, μ_{lin} and σ_{lin} decrease with increasing temperature due to phonon scattering, and band transport is the dominant transport mechanism, as is evident in Fig. 4.

At high temperatures greater than 340 K and high $V_{GS} - V_{ON}$ (high carrier densities), the μ_{lin} and the σ_{lin} decrease with increasing temperature due to phonon scattering, implying band transport. The values of σ_{lin} in this metallic region exceed 14 S/cm. At high tempera-

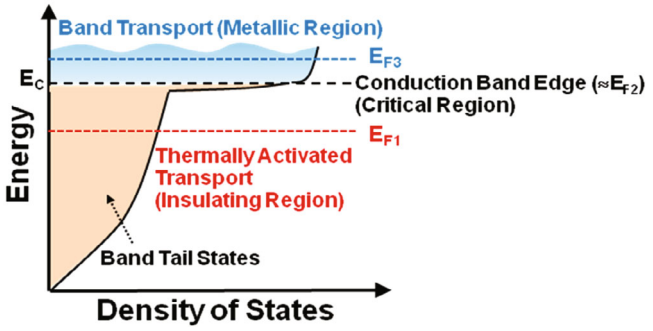

Fig. 6. (Color online) Schematic electronic structure of solution-processed ZTO deduced from the experimental results. It illustrates that an increasing gate voltage from V_{GS1} to V_{GS3} causes a shift of the Fermi energy level from E_{F1} to E_{F3}, gradually passing through the conduction band edge E_C ($\sim E_{F2}$), which indicates a transition from the insulating region to the metallic region passing through the critical region.

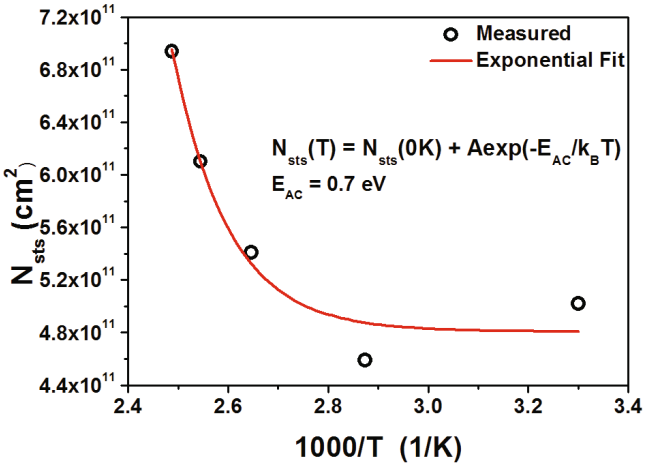

Fig. 7. (Color online) Temperature dependence of the subgap trap state, N_{sts}, obtained from the SS values listed in Table 1 by using Eq. (5). The exponential function $N_{sts}(T) = N_{sts}(0K) + Ae^{-(E_{AC}/k_BT)}$ was employed for the exponential fit, and the fitted result shows that the activation energy, E_{AC}, for N_{sts} at the E_F is 0.7 eV.

tures greater than 340 K and intermediate n_s (estimated to be 7.2×10^{11} cm^{-2} by using Eq. (3) and $V_{GS} - V_{ON} =$ 10 V), the mobility is approximately temperature independent. In this critical region, the mobility's decrease with increasing temperature due to phonon scattering is balanced by the apparent increase in μ_{lin} with increasing temperature due to the participation of more carriers in band transport. At lower n_s (lower $V_{GS} - V_{ON}$), the participation of more carriers in band transport dominates, and the μ_{lin} increases with increasing temperature. In this insulating region, thermally-activated transport is dominant.

The schematic electronic structure of solution-processed ZTO deduced from the experimental results is depicted in Fig. 6. Due to the amorphous nature of the solution-processed ZTO channel layer, band-tail states behave like electron traps. At low $V_{GS} - V_{ON}$ (low n_s) (Fermi level E_{F1}; insulating region), the E_F is energetically located within the band-tail, and only a small fraction of the carriers are transported in extended states through thermal activation, with MTR events defining the measured linear mobility. As the V_{GS} increases, localized states are filled with the V_{GS}-induced carriers, and the E_F moves toward the E_C. Thus, the E_{TAC} is reduced, and a larger fraction of carriers move into extended states at any given time (Fermi level E_{F2}; near critical region). Beyond a certain point ($n_s = 7.2 \times 10^{11}$ cm^{-2}, $V_{GS} - V_{ON} = 10$ V), the V_{GS}-induced carriers fill most of the localized states, and the E_F rises above the E_C. Carriers for the most part now move freely in the extended states, and band transport dominates (Fermi level E_{F3}; metallic region).

The MTR transport observed in these solution-processed ZTO TFTs has been reported for other material systems such as organic semiconductor crystals [22]. MTR transport, along with a conduction band edge, has also been assumed to be a possible transport mechanism in polycrystalline organic and polymeric semiconductor TFTs [14,23]. In this work, we found evidence for such transport in an amorphous solution-deposited ZTO.

An increase in the SS is known [24] to be related to an increase in the density of subgap trap states (N_{sts}) at the Fermi level that are located close to the semiconductor/insulator interface. This can be expressed by

$$N_{sts} = \left[\frac{SS \times \log_{10} e}{(k_B T/q)} - 1\right] \frac{C_{SiO_2}}{q}, \qquad (5)$$

where k_BT is the thermal energy and q is the elementary charge. Then, the temperature dependence of the N_{sts} data can also be obtained from the SS values listed in Table 1 by using Eq. (5) and is shown in Fig. 7. The low value of N_{sts} (5.02×10^{11} cm^{-2} at T = 303 K) indicates that the as-prepared TFTs developed in this study have a good ZTO/SiO_2 interface. The curve in Fig. 7 also shows that the N_{sts} has an exponential distribution. The exponential function $N_{sts}(T) = N_{sts}(0K) + Ae^{-(E_{AC}/k_BT)}$, where N_{sts} (0 K) is the N_{sts} value at T = 0 K, was employed for the exponential fit, and the fitted result is also illustrated in Fig. 7. The activation energy, E_{AC}, for the N_{sts} at the E_F obtained from the fitting procedure was 0.7 eV, which is similar to the E_{TAC} value of around 0.5 eV at $V_{GS} - V_{ON} = 1$ V as shown in Fig. 5.

IV. CONCLUSION

In this paper, we explore the charge-transport physics of solution-processed a-ZTO TFTs. We observe a range of charge-transport phenomena depending on the gate-voltage-dependent charge density in the a-ZTO channel

and on the temperature. For temperatures ranging from 348 to 402 K, the charge-transport mechanism transits from a thermally-activated to a band-like one with increasing V_{GS}, (*i.e.*, charge carrier concentration), and a clear conduction band edge is observed. We employed Maxwell-Boltzmann statistics in determining the E_{TAC} for shallow traps. The linear mobility-V_{GS} characteristics could be fitted well with an exponential distribution for the thermally-activated region, which results in a low E_{TAC} of less than 470 meV, and is strongly suggestive of MTR transport. Based on the experimental results, we also deduced the electronic structure of solution-processed ZTO, illustrating a transition from a thermally-activated (insulating region) to a band-transport (metallic region) behavior. The activation energy obtained from the temperature dependence of N_{sts} was closely related to the E_{TAC} value at low V_{GS}, suggesting that the subgap trap states are located in the range of 0.5 to 0.7 eV below the conduction band edge.

ACKNOWLEDGMENTS

This work was supported by the Industrial Strategic Technology Development Program (10041596, Development of core technology for TFT free active matrix addressing color electronic paper with day and night usage) funded by the Ministry of Trade, Industry & Energy (MI, Korea).

REFERENCES

[1] T.-J. Ha and A. Dodabalapur, Appl. Phys. Lett. **102**, 123506 (2013).
[2] C.-G. Lee and A. Dodabalapur, Appl. Phys. Lett. **96**, 243501 (2010).
[3] Y. B. Yoo, J. H. Park, S. J. Lee, K. M. Song and H. K. Baik, Jpn. J. Appl. Phys. **51**, 040201 (2012).
[4] Y. H. Hwang, S.-J. Seo, J.-H. Jeon and B.-S. Bae, Electrochem. Solid-State Lett. **15**, H91 (2012).
[5] C. G. Kim, N.-H. Lee, Y.-K. Kwon and B. Kang, Thin Solid Films **544**, 129 (2013).
[6] S. Dutta and A. Dodabalapur, Sens. Actuators B **143**, 50 (2009).
[7] S. Jeong, Y. Jeong and J. Moon, J. Phys. Chem. C **112**, 11083 (2008).
[8] C. H. Jung, J. Y. Lee, L. S. Pu and D. H. Yoon, Synthesis and Reactivity in Inorganic, Metal-Organic, and Nano-Metal Chemistry **41**, 1153 (2011).
[9] C. G. Lee, B. Cobb and A. Dodabalapur, Appl. Phys. Lett. **97**, 203505 (2010).
[10] W. Hu and R. L. Peterson, J. Mater. Res. **27**, 2286 (2012).
[11] K. Abe, N. Kaji, H. Kumomi, K. Nomura, T. Kamiya, M. Hirano and H. Hosono, IEEE Trans. Electron Devices **58**, 3463 (2011).
[12] N. Karl and J. Marktanner, Mol. Cryst. Liquid Cryst. **355**, 149 (2001).
[13] V. Podzorov, E. Menard, J. A. Rogers and M. E. Gershenson, Phys. Rev. Lett. **95**, 226601 (2005).
[14] V. Podzorov, E. Menard, A. Borissov, V. Kiryukhin, J. A. Rogers and M. E. Gershenson, Phys. Rev. Lett. **93**, 086602 (2004).
[15] P. G. Lecomber and W. E. Spear, Phys. Rev. Lett. **25**, 509 (1970).
[16] D. Monroe, Phys. Rev. Lett. **54**, 146 (1985).
[17] D. C. Paine, B. Yaglioglu, Z. Beiley and S. Lee, Thin Solid Films **516**, 5894 (2008).
[18] K. M. Yu, J. T. Yuh, S. H. K. Park, M. K. Ryu, E. J. Yun and B. S. Bae, Jpn. J. Appl. Phys. **52**, 10MA12 (2013).
[19] M. Debucquoy, S. Verlaak, S. Steudel, K. Myny, J. Genoe and P. Heremans, Appl. Phys. Lett. **91**, 103508 (2007).
[20] C. G. Lee, Ph.D. Dissertation, The University of Texas at Austin, May 2011.
[21] N. F. Mott, J. Phys. C: Solid State Phys. **20**, 3075 (1987).
[22] G. Horowitz, M. E. Hajlaoui and R. Hajlaoui, J. Appl. Phys. **87**, 4456 (2000).
[23] A. Salleo, T. W. Chen, A. R. Volkel, Y. Wu, P. Liu, B. S. Ong and R. A. Street, Phys. Rev. B **70**, 115311 (2004).
[24] T. Kamiya and H. Hosono, NPG Asia Mater. **2**, 15 (2010).